Using DAS to investigate traffic patterns at Brady Hot Springs, Nevada, USA

Kit Chambers[1]

https://doi.org/10.1190/tle39110819.1

Abstract

Although not as widespread as their use in other settings, there is a growing realization that distributed acoustic sensing (DAS) systems are suitable for traffic monitoring applications. One such application is demonstrated here using data from a surface DAS array recorded at Brady Hot Springs, Nevada, USA. Although this data set was acquired with the original intent of monitoring changes in a geothermal reservoir, it is shown that the data can also be used to identify and monitor vehicle movements on a nearby highway. Analysis of moveout patterns and recorded amplitudes confirm that this data set is dominated by signals generated by passing vehicles. During nighttime periods, the reduced traffic levels provide isolated signals that are more straightforward to analyze and interpret. During the day, however, increased traffic levels result in the signals from multiple vehicles overlapping to create a complex pattern of amplitudes recorded on the DAS array, making analysis and interpretation more challenging. Nonetheless, these signals can be separated and multiple vehicles identified along with their speeds and timings through the application of an automated workflow based on velocity stacking. The use of DAS for traffic monitoring purposes is an emerging technology, and despite challenges stemming from the nature of the measurement and the signals recorded, it can provide valuable information for the effective management of a transport network.

Introduction

The analysis of distributed acoustic sensing (DAS) data has the potential to revolutionize the management of transport networks, providing the ability to continuously monitor large areas at lower cost than competing technologies. As such, DAS analysis is a key component for developing smart city and smart infrastructure management. Within this sector, an emerging application for DAS is the monitoring of traffic patterns on roads and highways, where greater knowledge of vehicle traffic and road conditions form an important input for transport network management. Potential applications of DAS technology to traffic analysis include identifying hazards such as slow-moving traffic, stopped vehicles, or accidents, as well as providing information about wear and tear on the road surface.

One of the first published analyses of road traffic signals recorded on a DAS fiber was that of Martin et al. (2016), who found that vehicle traffic was a dominant noise source for a cable deployed alongside a road north of Fairbanks, Alaska. Similarly, Huot et al. (2017) identify different types of noise, including signals from vehicle traffic, using DAS recordings. In another study, Liu et al. (2018) analyze the signals from passing vehicles on DAS fibers. Using a wavelet threshold algorithm, they developed procedures for noise attenuation as well as analysis of vehicle counts and speeds. In a slightly more novel application, Wang et al. (2020) use a section of underground fiber to detect and analyze traffic from a parade through Pasadena, California. The results identify signals from individual parade floats and show periods of congestion. Lancelle (2016) and Feigl and Parker (2019) discuss two applications of DAS to vibrations caused by passing vehicles. The first utilized a 750 m deployment at Garner Valley, California, where the authors were able to track the speed and position of vehicles. The second example used the DAS array from Brady Hot Springs, Nevada (the same site analyzed here), however, analysis was somewhat limited, using only a small subset of the sensors (approximately 250 of 8621 sensing segments) for a 1-hour period. Nonetheless, these results hint at the capability of DAS to monitor vehicle activity and traffic patterns. Traffic monitoring applications of DAS have also been discussed by Jousset et al. (2018), Lindsey et al. (2020), and Yuan et al. (2020). These studies have found the traffic signal to be dominated by a low-frequency (less than 1 Hz) quasi-static component that can be used to evaluate ground properties. Finally, the noise from traffic can also be combined with techniques such as seismic interferometry to gain information about the subsurface. For example, both Matzel et al. (2017) and Feigl and Parker (2019) describe experiments where traffic noise constituted a significant part of the ambient noise field for the construction of interferometric Green's functions.

Here, I demonstrate the applicability of DAS data for traffic monitoring using a historical and freely available data set collected at the Brady Hot Springs geothermal project (Feigl and Parker, 2019). To date, the analysis of these data has primarily focused on their integration with other data sets to provide increased resolution and a combined interpretation for the mechanical behavior of both rock and fluids in the geothermal reservoir (Patterson et al., 2017; Feigl, 2018; Miller, 2018; Feigl and Parker, 2019). Here, I take a different approach. Using signals from what normally would be considered extraneous surface noise sources, I expand upon the work presented in Feigl and Parker (2019) to illustrate the potential of DAS fibers for traffic monitoring. In particular, I provide analysis of the vehicle signals without reference to arrivals on individual recordings. As such, the procedure can be applied when the DAS data are noisy, and it provides a method for separating the signals from multiple vehicles during heavy traffic when the signals overlap. Finally, I describe and apply a processing flow to detect and analyze traffic during two 7-hour data segments. Although the

[1]Motion Signal Technologies, St. Newlyn East, UK. E-mail: kit.chambers@motionsignaltechnologies.com.

results are preliminary, they show the potential of combining DAS systems with geophysical processing techniques to gain information about traffic movements.

Horizontal DAS at Brady Hot Springs

In March 2016, the Brady Hot Springs geothermal project was the site of a major and multifaceted geophysical survey — the PoroTomo project. Elements of the study included active seismic sources, fiber-optic cables for DAS and distributed temperature sensing (DTS), 246 three-component seismometers, and pressure sensors in observation wells. (For details, see Miller [2018] or Feigl and Parker [2019].) Four separate fiber-optic systems were installed to record DAS and DTS data in a vertical borehole array to a depth of approximately 400 m and a horizontal array deployed at the surface (Mondanos and Coleman, 2018).

Here, the focus is on analysis of the DAS data from the horizontal near-surface array deployed at Brady Hot Springs. The array layout is shown in Figure 1 and consists of approximately 8700 m of fiber-optic cable buried in a trench 0.5 m deep. Data were recorded for about 15 days during which hydraulic conditions in the subsurface were intentionally manipulated. The data were collected using sensing segments spaced at 1 m with a 10 m gauge length. As described by Miller (2018) and Mondano and Coleman (2018), the acquisition system recorded radians optical phase per second, which through the application of scalar gain can be converted to nano-strain rate.

As can be seen from Figure 1, the array is in the vicinity of several potential sources of anthropogenic signals. In addition to buildings and infrastructure, there is a major highway (I-80, the Dwight D. Eisenhower Highway) 50 m from the western edge of the array. There is also a frontage/service road running through the center of the array.

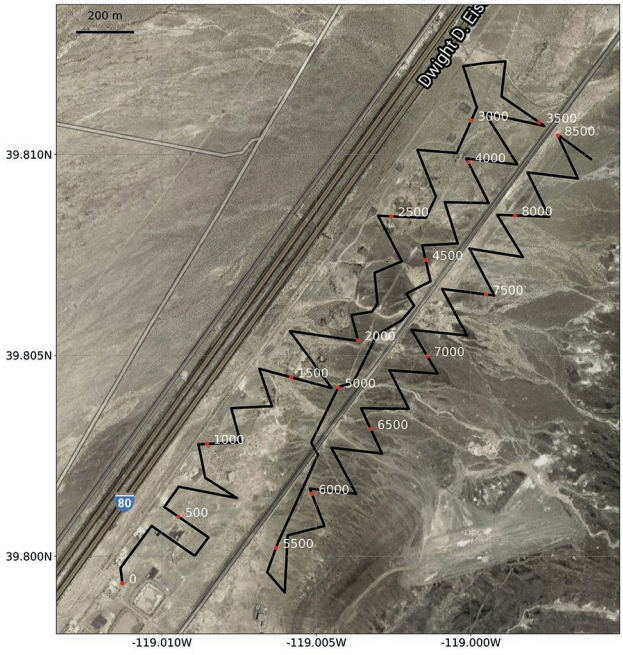

Figure 1. Map of the horizontal DAS array deployed at Brady Hot Springs with aerial photo/satellite image background. The black line denotes the DAS cable, and the position of every 500th sensor is marked. Note that there is a major highway approximately 50 m west of the array and a frontage road running though the center of the array.

Fifteen days of data were collected; however, not every time period is suitable for traffic analysis due to the presence of active-source acquisition during the deployment. During vibroseis sweeps, the signal recorded on the DAS fiber is dominated by the associated ground roll. As such, care was taken to select data segments during which active seismic was not being recorded.

Traffic signals recorded at Brady Hot Springs

To begin, I examine the DAS recordings for two 7-hour segments. The waterfall plots in Figure 2 show root-mean-square (rms) amplitude recorded by the whole array in 15 s time windows. Several features are noticeable from the data. For example, there is a horizontal band of high amplitudes recorded near sensor 4750. This is due to the cable being deployed on the ground rather than trenched in this location (K. L. Feigl, personal communication, 2020). The same is true for some other areas with consistently high amplitudes, such as near the cable start (sensors 0–200 approximately).

In general, as would be expected from anthropogenic sources, amplitudes are typically higher during the day (Figure 2a) compared to night (Figure 2b). Furthermore, the energy is organized into thin near-vertical bands (i.e., short time, large spatial extent bursts). These vertical bands have higher amplitudes on sensors 0–4000 compared to those farther down the fiber. Notably, it is these sensors (0–4000) that are closer to the highway running down the western edge of the array, and the near-vertical bands are also less dense in time during the night (Figure 2b). These observations are consistent with the high-amplitude near-vertical bands being due to vibrations from vehicle traffic on the highway, as we would expect highway traffic to produce larger amplitudes on sensors closer to the highway and reduced activity during the nighttime hours. It also seems likely that the signals extending to higher channel numbers in Figure 2a (for example around time 2016/03/14 16:45 UTC-6) are related to traffic on the frontage/service road, as these signals produce high amplitudes on sensors on the far side of the array from the highway.

Properties of vehicle signals

In general, the signals from vehicles are highly variable between sensors due to a number of factors, including the variable orientation of the fiber, the complex nature of the moving source, and the variable coupling of the ground motion to the sensing fiber. There are, however, some general properties of the vehicle signals that we can use to better isolate and interpret traffic patterns.

Figures 3a and 3b show an example recording from sensor 1000 taken during the night with a single dominant vehicle signal. Figure 3a shows the time-frequency spectrum evaluated over 10 s overlapping windows, whereas Figure 3b shows the original time series. Notably, and in contrast to previous traffic observations using DAS (Jousset et al., 2018; Lindsey et al., 2020; Yuan et al., 2020) the signal is not dominated by a low-frequency (quasi-static) component. Instead, the emergent 10 s pulse contains spectral peaks just above 10 and 20 Hz with the majority of the energy in the sub-30 Hz band.

The reason for the absence of the low-frequency component in the Brady Hot Springs data is most likely due to the increased distances and the rapid amplitude decay with distance for the quasi-static signal. For example, at Brady Hot Springs the distance from the sensors to the road is on the order of 50–250 m, whereas the studies observing the quasi-static component of the signal use offsets less than 7 m (Jousset et al., 2018; Lindsey et al., 2020; Yuan et al., 2020). Instead, the pulse in Figure 3 is most likely surface-wave energy from the moving vehicle source. Surface-wave arrivals from vehicle sources also are observed by Yuan et al. (2020), who note that they dominate the vibration signal at greater distances. Unlike the quasi-static pulse, which has an amplitude decay inversely proportional to distance, surface waves have an amplitude decay inversely proportional to the square root of distance. As such, surface waves are expected to dominate the observed wave train at longer offsets, such as those used here.

One curious (and consistent) feature for the vehicle pulse in Figure 3 is the energy peaks transitioning to lower frequency over the duration of the pulse. For example, the 20 Hz peak starts off closer to 25 Hz at the start of the pulse. This pattern of frequency decay is the opposite of what would be expected from surface-wave dispersion effects because in the presence of dispersion we would expect the lower-frequency components to arrive earlier. The signal switching between dominant surface-wave mode branches may cause the observed frequency shift. However, an alternative possibility is that this frequency change is caused by a Doppler shift. This would result in arrivals from a moving source being observed with a higher apparent frequency while the source is traveling toward the sensor. Then, as the source passes the sensor, there is a decrease in observed frequency. Finally, the arrivals are observed with a lower apparent frequency as the source moves away from the sensor. The observed shifts (approximately 2 Hz for the 10 Hz band and 4 Hz for the 20 Hz band) are consistent with a vehicle moving at 29 m/s (the average speed for cars on the highway) at an offset of 50 m from the receiver (the approximate distance of channel 1000 from the road) and a medium speed of 300 m/s.

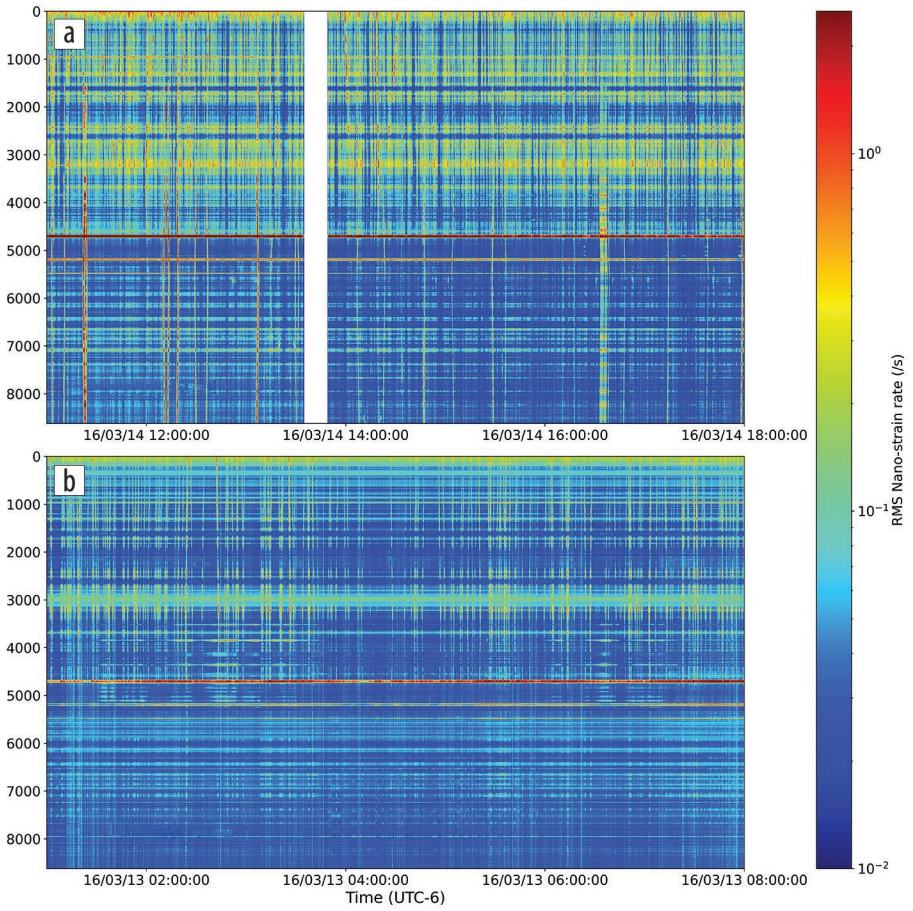

Figure 2. Root mean square computed for 15 s time windows for two 7-hour time periods. (a) Daytime activity. (b) Nighttime and early-morning activity. Sensor numbers correspond to the labels in Figure 1. As such, the higher levels of activity on sensors 0–4000 correspond to the sensors closer to the highway west of the array.

Data compression

The large number of measurement points and continuous recording of DAS systems enable them to generate large data volumes. As such, data compression procedures are an important part of DAS analysis as they provide increased storage capacity and processing efficiency by reducing network throughput.

Figure 3 shows the results of a compression algorithm applied to the vehicle signal. Figures 3a and 3b (discussed in the previous section) show the original data trace, and Figures 3c and 3d show the same trace after treatment with a compression algorithm.

The compression algorithm is based on a wavelet packet transform (see Foster et al. [1994] or Wu et al. [2006]) of segments 256 samples long for each trace. The resulting coefficients are then discretized using the minimum number of levels to guarantee a relative rms misfit of 99% to the original data. As such, the compression algorithm is lossy, and the amount of compression provided is variable depending on data content. However, the compression does not significantly change the vehicle pulse (Figure 3d). Rather, the result of the compression is to attenuate some of the noise observed in the time-frequency plot (Figure 3c). When applied to data segments from Brady Hot Springs, typically 80%–85% reduction in data volume is achieved, which translates to substantial computational and storage savings when analyzing these data.

Band-limited analysis of vehicle signals

While useful for providing a data set overview, the rms 15 s average presented in Figure 2 is too coarse to provide much information regarding vehicle movements. Similarly, inspecting individual traces (Figure 3) is not practical for the thousands of

sensors in the Brady DAS array. As such, a compromise is to compute the average amplitudes in discrete frequency bands for short time windows.

Figures 4 and 5 show average frequency amplitudes in the 5–30 Hz range over 5 s time windows. This frequency band and window length were chosen to maximize energy from the vehicle signal and demonstrate the moveout of vehicle signals across the array, while also making the processing and examination of large time segments practical.

The half-hour time segment shown in Figure 4 was taken during the nighttime and as such contains fewer superposed signals, making it simpler to interpret. Based on the moveout patterns, the majority of the larger signals appear to be from sources moving from northeast to southwest along the highway. Notably, vehicles moving northeast to southwest would be on the far side of the highway from the DAS array. The fact that they produce larger signals in this data segment could be due to these being larger sources (i.e., trucks rather than cars). It is also worth noting that although the signals are stongest on the sensors closest to the highway, in many cases they can be tracked across the entire array up to several hundred meters from the source.

Figure 5 also shows averages of the 5–30 Hz band over a half-hour time segment. In this case the time segment takes place during the day and we observe a significant increase in activity with many of the signals from different vehicles merging together to create a complex pattern on sensors 0–3500. There are also two examples of signals with high amplitudes extending across the entire array (at around 15:05 and 15:28). Comparison of these anomalies with the sensor positions (Figure 3b) confirms that these signals originate from the frontage/service road.

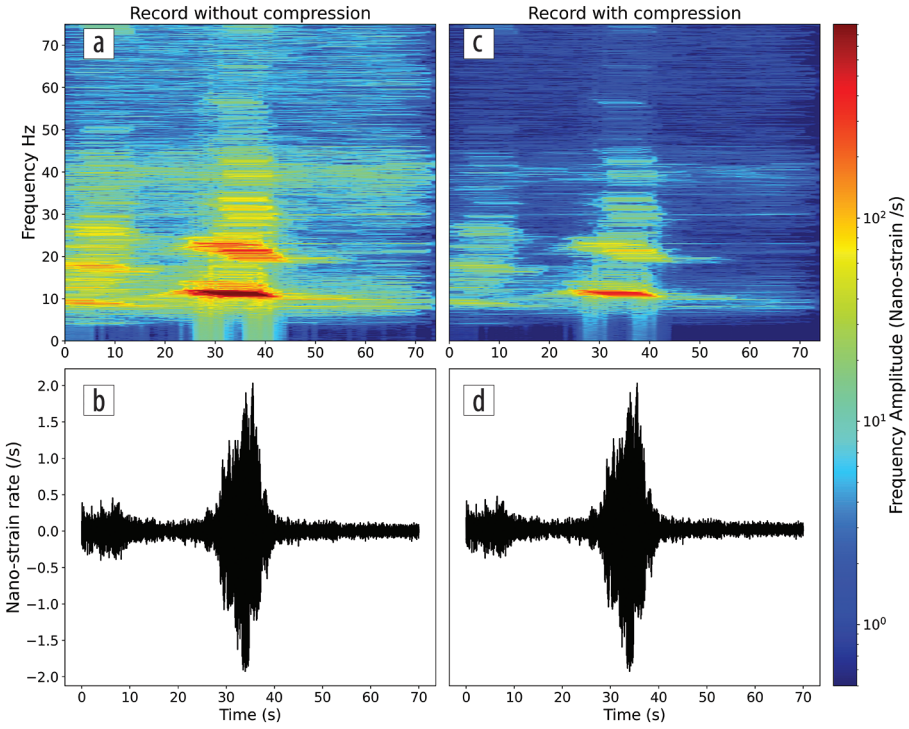

Figure 3. Waveform examples for a vehicle observed at sensor 1000. (a) Time-frequency spectrum computed using overlapping 10 s windows. (b) Corresponding time series. Panels (c) and (d) are the same but use compressed data.

Separating vehicle signals during heavy traffic periods

Having established some broad properties of the traffic signals in the DAS data from Brady Hot Springs, I now turn attention to a processing flow for isolating

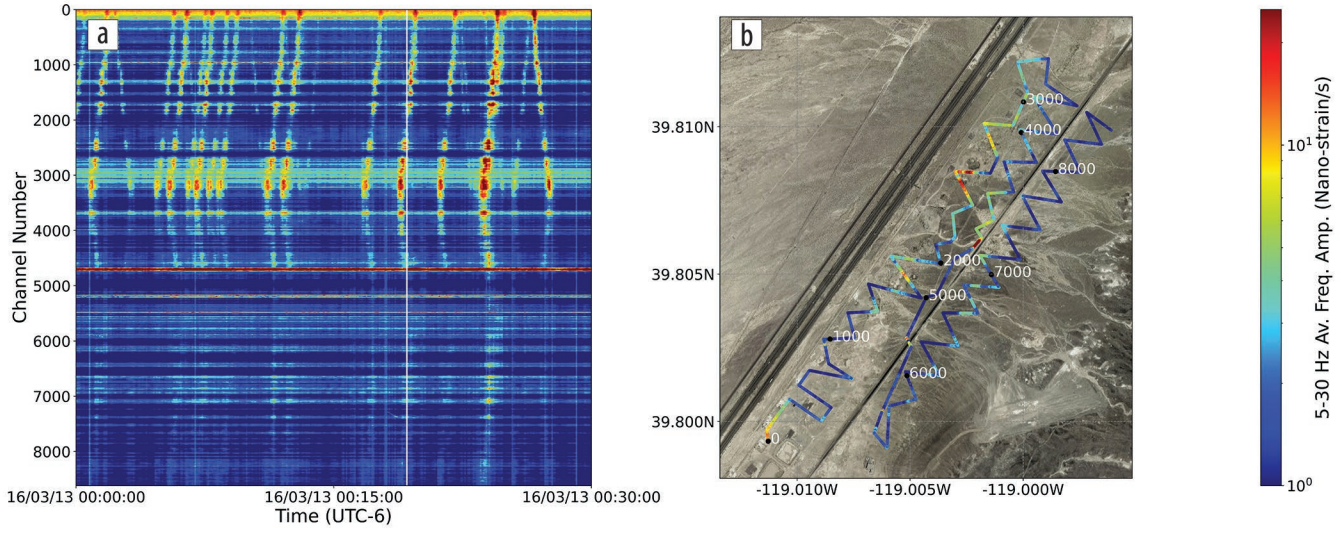

Figure 4. (a) Average of the 5–30 Hz amplitude spectrum in 5 s windows for a half-hour time segment during the nighttime. Panel (b) shows a time slice (denoted by the white line in [a]) projected on to the sensor positions. The reduced traffic at night allows the identification of individual vehicles.

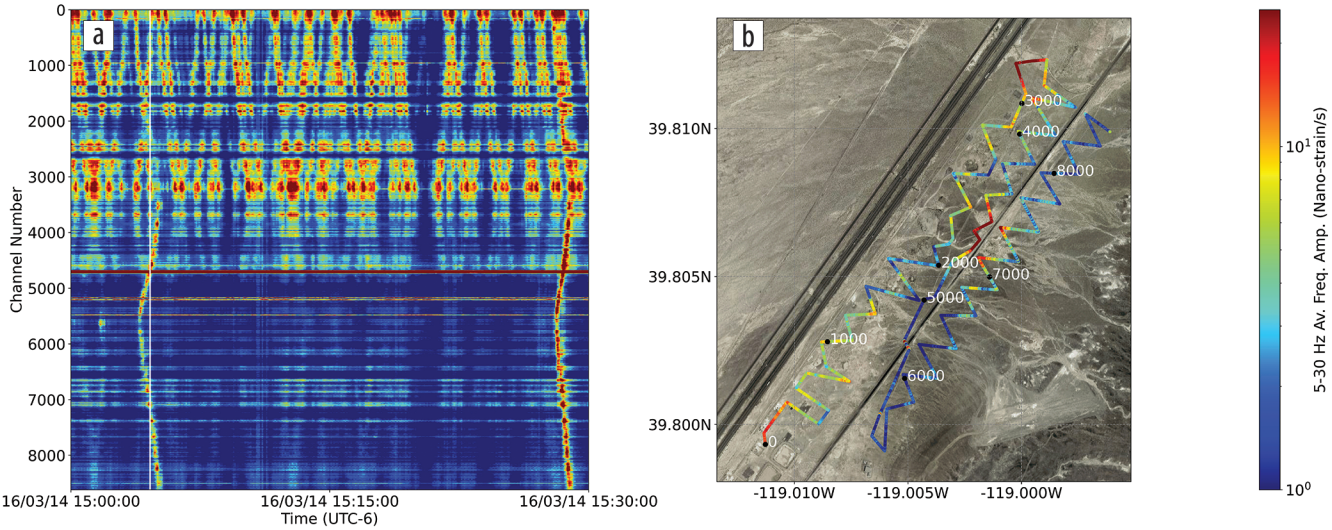

Figure 5. Same as Figure 4 but for a half-hour time segment during the day. The overlapping of arrivals from multiple vehicles on the highway produces a complex pattern on sensors 0–4000. The map projection in (b) also shows that high-amplitude signals extending beyond sensor 5000 are consistent with traffic on the frontage road trending through the center of the array rather than the highway to the west.

vehicle signals during periods when the arrivals from multiple vehicles overlap. The method contains two steps: first, signal processing techniques are applied to further enhance the arrivals; second, the overlapping signals are separated by a stacking or beamforming procedure based on the vehicle velocity.

To demonstrate the processing, I consider data from a subset of 3665 of the sensors closest to the road and use a rotated sensor geometry such that the *x*-axis is aligned with the road (Figure 6a). While a rotated coordinate system is not strictly necessary for the processing, it makes the analysis simpler, allowing us to consider vehicle velocity in a single direction. The subset of sensors was determined after analysis of a variety of different geometries and was chosen to minimize the trade-off between gaining greater stack power by including more sensors in the beamforming and reduced signal-to-noise ratio resulting from the inclusion of sensors farther from the road.

The goal of the signal preprocessing sequence is to enhance the visibility of the arrivals from vehicles as well as mitigate some of the effects from the complex source and cable geometry. The sequence is as follows:

1) subtraction of a median trace to remove zero moveout noise across the array that Feigl and Parker (2019) attribute to vibrations of the interrogator unit
2) removal of frequency spikes with an FX median filter (see Chambers and Booterbaugh [2018])
3) frequency band pass from 5 to 30 Hz
4) construction of signal envelopes from the traces (This removes expected polarity reversals due to a changing fiber orientation relative to the source and mitigates some of the effects of surface-wave dispersion. The use of signal envelopes also has the effect of lowering the effective frequency content of the pulse, thus reducing the sensitivity of subsequent stacking operations to variations in road to sensor distance.)
5) smoothing using a moving Gaussian average with sigma of 0.125 s

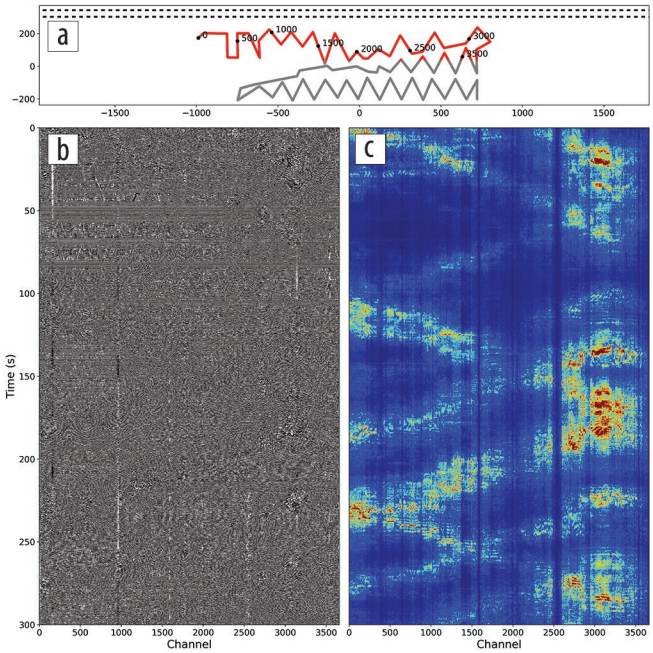

Figure 6. (a) Map of the horizontal DAS array in rotated coordinates such that the *x*-axis is parallel to the highway. The sensors used in (b) and (c) are marked in red and numbered. Horizontal dashed lines show the position of the near and far lanes of the highway. (b) Five minutes of raw data corresponding to the selected sensors. Data have been corrected for bias, but otherwise no other processing has been applied. The origin of the time axis is 2016/03/04 15:10 (UTC-6). (c) Data segment from (b) after application of the preprocessing sequence described in the text. The vehicle signatures now can be seen as linear features crossing the array.

Figures 6b and 6c show the effect of the preprocessing on a 5-minute time segment of data. As can be seen from the figure, multiple vehicle signals that are not identifiable in the raw data can be observed in the preprocessed data. In the preprocessed data, it is possible to track the signals from vehicles across the array. Nonetheless, the data still contain noise, and the signals

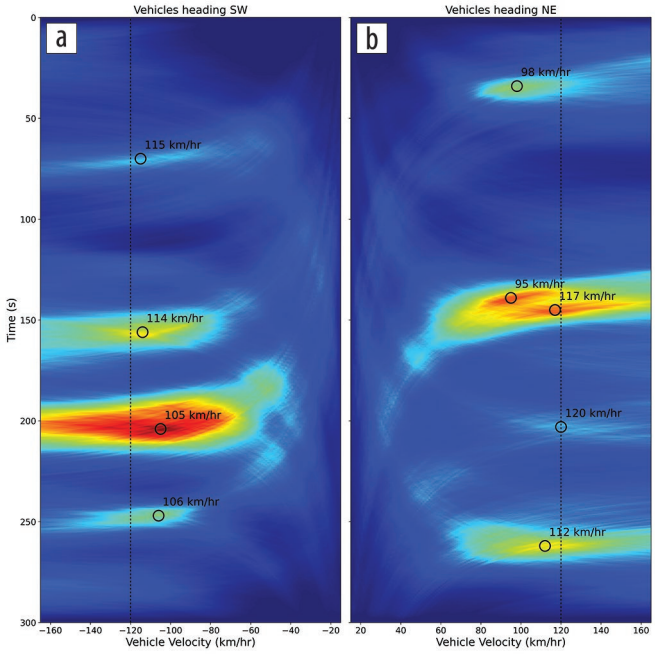

Figure 7. Velocity stacks for the 5-minute processing segment shown in Figure 6. (a) Stacks for vehicles heading southwest on the highway (i.e., negative *x*-direction in the rotated coordinate system). (b) Stacks for vehicles heading northeast on the highway (i.e., positive *x*-direction). The timing and speeds of nine vehicles are marked with open circles. For reference, the vertical dashed lines at +/–120 km/hour (i.e., 75 miles/hour) denotes the Nevada state speed limit for rural highways. Vehicle velocity moveout is computed relative to the origin of the *x*-axis in the rotated coordinate system, hence the timing of vehicle signals refers to their times at the nearest point on the road to the array center.

are complex with the arrivals from several different vehicles superimposed on top of each other.

Figure 7 shows the application of velocity stacking to the 5 minutes of data from Figure 6c. As the name suggests, velocity stacking is based on aligning the data for different speculative vehicle velocities and computing a stack function. In this case, the stacking function consisted of a semblance weighted stack followed by a time domain Gaussian smoothing operator (with sigma 0.05 s).

The principle of velocity stacking is based on response from a moving vehicle being a superposition of signals generated by the vehicle at each time and position along its path. In the case in which an array of sensors is deployed parallel to the path/road, a vehicle moving at a constant velocity will produce a planar arrival with a slope corresponding to the vehicle's velocity that is offset from the origin. The offset time of the arrival, T_0, is a function of the distance to the road as well as subsurface properties. By computing synthetics for a range of different fiber offsets, a calibration curve of T_0 versus fiber offset was generated and then used to correct for time shifts on sensors at different distances from the road. The modeling used a homogenous half-space with a surface-wave velocity of 300 m/s and attenuation factor (Q) of 50. The medium velocity was chosen to be consistent with the lower end of values for shear-wave velocity in the near surface given by Zeng et al. (2017). The signal from the moving vehicle was modeled assuming four point forces corresponding to a chassis length of 2 m and axle length of 1.5 m traveling at 30 m/s parallel to the sensing array. For the receiver distribution used at Brady Hot Springs, it was found that the maximum time correction required was 0.13 s. This is an order of magnitude less than the typical pulse length in the preprocessed data. As such, the first-order control on the pulse moveout is determined by the vehicle velocity.

From Figure 7, it can be seen that instead of plotting as superposed plane waves, the signals from multiple vehicles separate in the velocity-time domain to produce several distinct peaks, each corresponding to a traveling vehicle. From the data segment presented, it is possible to identify the signals from nine different vehicles — four traveling southwest on the far side of the highway and five traveling northeast on the near side.

The strongest signal is for a vehicle traveling at 105 km/hour to the southwest. Notably, this signal has both the highest amplitude and the longest time-duration anomaly in this data segment. The stack function amplitude or brightness is a function of both the input signal amplitudes and their coherency across the data set. As such, the longer duration and higher amplitude of this anomaly is probably due to it being the result of a larger vehicle such as a truck rather than a car.

The weakest anomaly and hence least robust of the vehicles observed in Figure 7 is the signal consistent with a source traveling at 120 km/hour to the southwest. As can be seen from the figure, the anomalies' diffuse nature in this case makes speed estimation difficult, and further work is required to isolate this signal. However, the position of the vehicle's anomaly in the velocity-time stack suggests it was traveling close to or in excess of the Nevada speed limit for rural highways, which is 75 miles/hour or 120 km/hour.

A final feature worth noting from Figure 7 is the closely spaced vehicles traveling at 95 and 117 km/hour to the northeast. In the preprocessed data (Figure 6c), it is difficult to distinguish these arrivals from each other. However, the velocity-time stacking successfully separates these two features, thus demonstrating the applicability of this technique for the analysis of busy traffic periods.

Automated traffic analysis

The velocity stacking technique can be incorporated into an automated processing flow for vehicle detection and traffic analysis. I now demonstrate an example of such a workflow using the two time periods shown in Figure 2, corresponding to 7 hours of daytime activity and 7 hours of nighttime activity, respectively. In each case, the time period was divided into 5-minute segments for processing with 30 s overlap between segments to allow for vehicle signals near the start and end of segments. The data segments were each subjected to the preprocessing sequence and velocity stacking technique described in the previous section. Up to 200 local maxima were then selected from the velocity stacks for each 5-minute time window as potential vehicle identifications.

Figure 8 shows the time and stack amplitude for selected maxima for both time periods. The distributions for both day

and night segments are characterized by having relatively few high stack amplitude anomalies with a cluster of low amplitudes. These low amplitudes are effectively a noise floor, and the higher-amplitude candidate vehicle signals can be separated using a threshold criterion. Because the noise floor varies over time, it is desirable to use a data-adaptive threshold to separate the candidate vehicle signals. Here, I use the median of the stack amplitude computed over 10-minute windows plus a user-determined shift of 0.048 times the maximum stack amplitude value detected over both time periods (i.e., threshold = median + 0.048 * max amplitude). This technique has the advantage of allowing for variable noise levels as well as periods in which there are no vehicle signals.

Figure 9 shows the velocity and times for the candidate vehicle identifications. In total, 1530 and 458 anomalies are selected by the threshold criterion for day and night periods, respectively. Although the amplitude thresholding reduces the number of anomalies, there is still potential for false positive vehicle detections. For example, activity on the frontage road through the center of the array, other noise sources, or crosstalk between signals in the velocity stacking all could produce spurious signals that would be classed as potential vehicle observations. However, these signals will in general create anomalous vehicle observations compared to the dominant source of traffic from the highway. This can be seen by considering the distribution of observed velocities (Figure 9), which for both time periods and directions of travel is characterized by a relatively dense central band with outliers having very high or low velocities. In Figure 9, these outliers are defined as anomalies with a velocity less than 75 km/hour or greater than 135 km/hour. Excluding these outliers provides the set automated high-confidence vehicle detections.

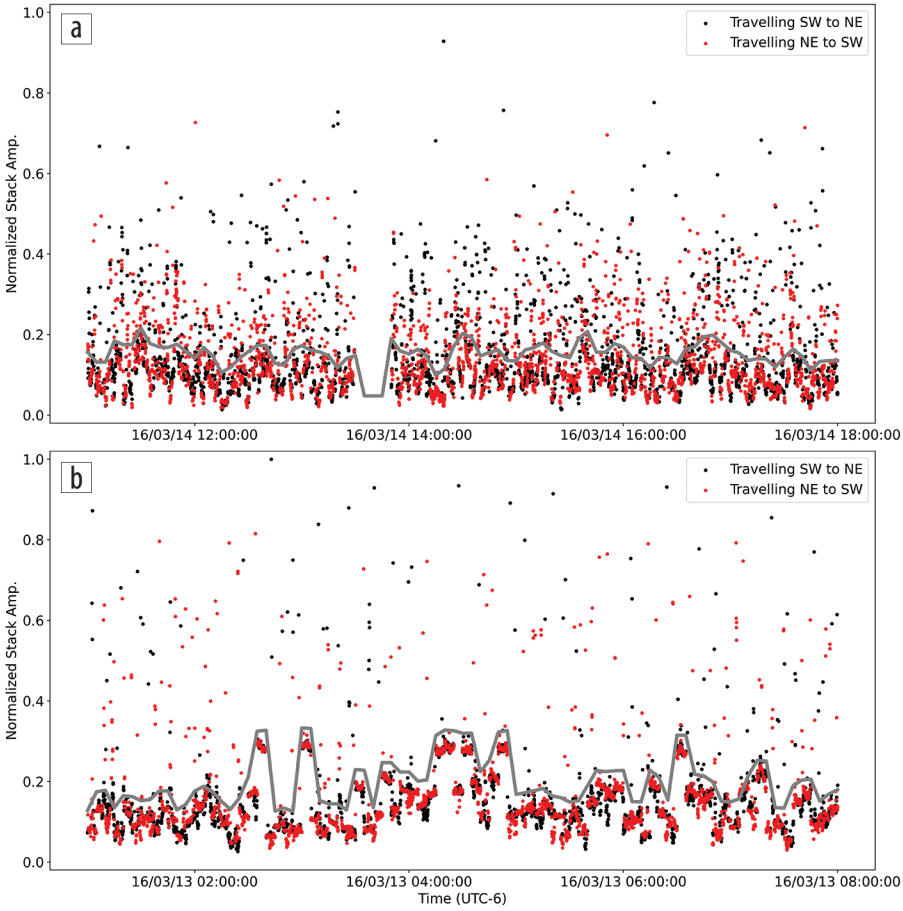

Figure 8. Stack amplitudes and time of local maxima identified from the velocity stacking as part of the automated workflow. (a) Maxima identified on the 7 hours of daytime data considered. (b) The same but of the 7 hours of nighttime data considered. Stack amplitudes are normalized by the largest value detected over both time windows. The gray line is the adaptive threshold used in processing, computed as the median stack amplitude over a 10-minute window plus 0.048 times the maximum amplitude over both time windows.

Table 1 summarizes the detection results for the two time segments and directions of travel. In total, 1322 vehicles were detected over the 14 hours of data analyzed. Of these, the majority 76% (1007) were traveling during the daytime period. The distribution of vehicle directions is less asymmetric with just under half (614 or 46%) traveling from southwest to northeast. Average speeds are consistent between the different times and directions of travel, with the exception of vehicles traveling at night from southwest to the northeast being slightly faster. The observed average velocity difference for vehicles traveling southwest to northeast at night is small, however, and it remains to be seen if this is significant. Figure 9 also provides an indication of the vehicle rate, which is fairly consistent for the daytime period (approximately 2.4 vehicles/minute). However, during the nighttime segment there are periods of reduced activity, such as between 04:00 and 05:00. There is also a burst of activity going both directions just after 07:00. This may be due to increased traffic on the frontage road through the center of the array rather than on the main highway. Feigl and Parker (2019) note a period of increased activity associated with vehicles traveling to a quarry in the early mornings. However, 13 March 2016 was a Sunday, which makes this less likely, and frontage road activity is not apparent in the waterfall plot covering this time (Figure 2b). Inspection of the velocity stacks and preprocessed data for this time period show two clear vehicle signals consistent with highway traffic, with several other arrivals close to the detection threshold.

Discussion and conclusion

Although the DAS data set at Brady Hot Springs was not designed with traffic monitoring in mind, it has proven to be a useful resource for developing and demonstrating the potential of DAS arrays for traffic analysis. In fact, analysis of the

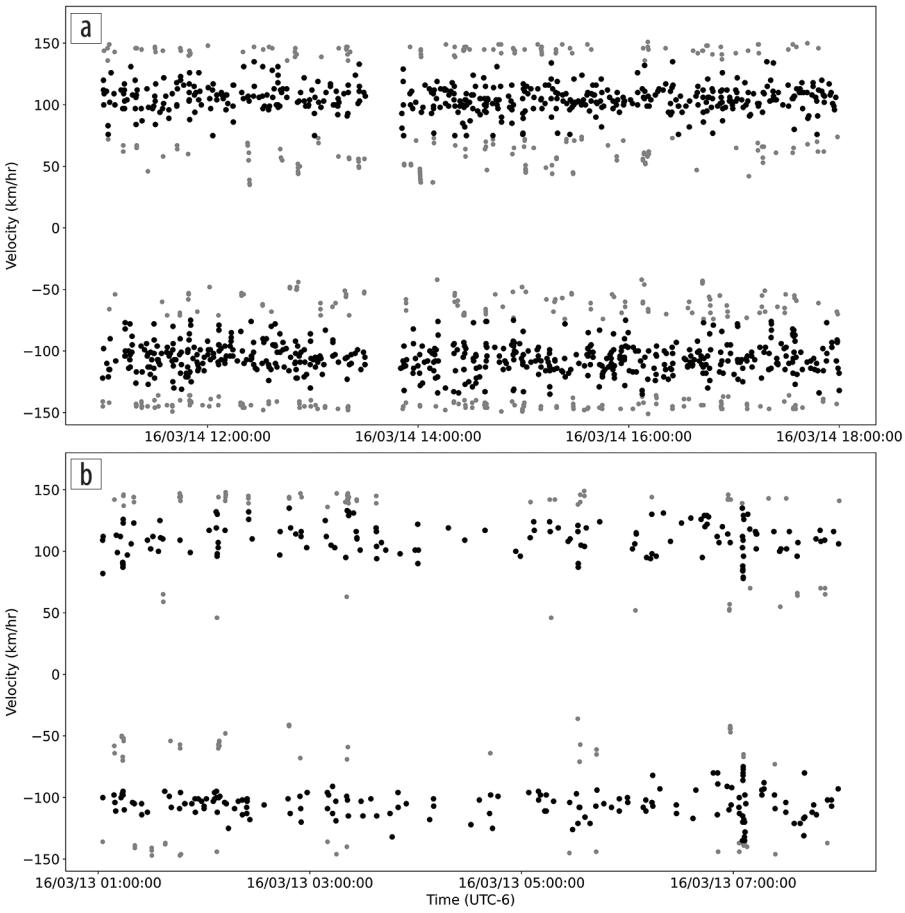

Figure 9. Vehicle observation times and velocities for the two 7-hour sections of data examined during (a) daytime and (b) nighttime. Black points are the high-confidence observations obtained after the removal of the outliers (gray) based on the vehicle velocity.

Table 1. Results of the automated vehicle processing workflow. Maxima refers to the number of local maxima identified in velocity stacks. Candidate vehicle identifications refers to the number of observations remaining after the stack amplitude thresholding described in the text. Vehicle observations are those results remaining after removal of the velocity outliers.

	Maxima	Candidate vehicle identifications	Vehicle observations	Average speed (km/hr)
Day traveling SW–NE	3149	713	468	104
Day traveling NE–SW	3163	817	539	–105
Night traveling SW–NE	4872	222	146	110
Night traveling NE–SW	4772	236	169	–105

distribution of amplitudes and moveouts of energy across the array shows that this data set is dominated by signals generated from passing traffic.

The observed signals from vehicles are most likely surface waves excited by the passing traffic and can be observed at several hundred meters from the highway (on the other side of the array) in some cases. This in turn makes a case for the analysis of surface waves being able to increase the monitoring range from DAS fibers compared to analysis of low-frequency (quasi-static) components of the wavefield.

The rms and frequency band analysis both show, unsurprisingly, that traffic levels on the highway are reduced during nighttime periods. Meaning that, during the night, these signals are typically isolated and easily identified. However, during the day, traffic levels on the highway are such that the arrivals from multiple vehicles can overlap. In these periods, time-velocity stacks can be used to separate the arrivals from individual vehicles and provide their time and speed.

The analysis presented here demonstrates the potential of DAS data to analyze and monitor vehicle traffic on roads. Nonetheless, there is scope for future work in multiple areas on this topic, including the optimization of preprocessing strategies, the robustness of the velocity stacks, the selection of vehicle signals, and the analysis of the error/precision of vehicle velocity measurements. Further work also could consider the influence of surface-wave dispersion in the context of wavefields generated by moving sources. In the present work, the effects of surface-wave dispersion are mitigated through the application of the signal envelope in preprocessing. However, more detailed studies in the future may need to take this phenomenon into account to achieve higher resolution. Increased resolution would enable the separation of closely spaced vehicles traveling at the same speed. In fact, this could be the case for the largest anomaly observed in Figure 7.

It is also worth noting that the vehicle velocity derived from the time-velocity stacks is an apparent velocity. Although the rotated coordinate system used for the stacking minimizes this error, calibration using vehicles with known speeds may be required to establish true vehicle velocity in some cases. Improvements in acquisition technology will also facilitate traffic analysis. Since the time that the data set at Brady Hot Springs was collected, interrogator technology has improved, resulting in an order of magnitude increase in signal-to-noise ratio (Feigl and Parker, 2019).

Although the automated vehicle detection procedure is described here using an existing data set, the procedure can be applied equally in real-time monitoring scenarios. Besides the preprocessing settings, only two additional parameters are used in the automated vehicle identification — the threshold shift

criterion and the range for reasonable vehicle velocities — and all input parameters can be adjusted on the fly if necessary. The large data volumes associated with DAS acquisition also make computational resources a key consideration. This is particularly true if processing is to be performed near the acquisition unit, in which case power consumption is often a key constraint. However, the application of data compression allows for efficient transfer of the DAS data to external/cloud computing facilities for analysis. Although the processing sequence described here does not have a large computational footprint (compared to many seismic processing operations), it is easily parallelized.

DAS is an attractive alternative to many traditional traffic monitoring technologies due to its lower installation and maintenance cost and its less-intrusive nature. However, this application of fiber-optic sensing is still an emerging technology, and numerous issues must be overcome before its widespread adoption. Issues such as the large data volumes, instrument noise, complex nature of the sources, directionality of the DAS measurement, and coupling of the ground movement to the fiber all make these challenging data sets to analyze. Nonetheless, overcoming these challenges can provide an important ingredient in the delivery of safer and more efficient transport networks. TLE

Acknowledgments

The author would like to thank the leaders of the PoroTomo project for making the data at Brady Hot Springs publicly available and Kurt Feigl for providing additional information on the DAS deployment. The author would also like to thank Ray Chambers, Phil Winder, Yunyue Elita Li, an anonymous reviewer, and the associate editor Ariel Lellouch for constructive suggestions that improved this manuscript.

Data and materials availability

The Geothermal Data Repository provides links to the DAS waveform data and associated metadata at https://gdr.openei.org/submissions/980.

Corresponding author: kit.chambers@motionsignaltechnologies.com

References

Chambers, K., and A. Booterbaugh, 2018, Improving microseismic data quality with noise attenuation techniques: GeoConvention, CSEG, https://bit.ly/3ii8crv, accessed 1 October 2020.

Feigl, K. L., 2018, Overview and preliminary results from the PoroTomo project at Brady Hot Springs, Nevada: Poroelastic tomography by adjoint inverse modeling of data from seismology, geodesy, and hydrology: Proceedings of the 43rd Workshop on Geothermal Reservoir Engineering, Stanford University, https://stanford.io/3iMGUtD, accessed 9 October 2020.

Feigl, K. L., and L. M. Parker, 2019, PoroTomo final technical report: Poroelastic tomography by adjoint inverse modeling of data from seismology, geodesy, and hydrology: U.S. DOE Office of Energy Efficiency and Renewable Energy, Geothermal Technologies Office, technical report, https://doi.org/10.2172/1499141.

Foster, D., J., C. C. Mosher, and S. Hassanzadeh, 1994, Wavelet transform methods for geophysical applications: 64th Annual International Meeting, SEG, Expanded Abstracts, 1465–1468, https://doi.org/10.1190/1.1822812.

Huot, F., Y. Ma, R. Cieplicki, E. Martin, and B. Biondi, 2017, Automatic noise exploration in urban areas: 87th Annual International Meeting, SEG, Expanded Abstracts, 5027–5032, https://doi.org/10.1190/segam2017-17774369.1.

Jousset, P., T. Reinsch, T. Ryberg, H. Blank, A. Clarke, R. Aghayev, G. P. Hersir, J. Henninges, M. Weber, and C. M. Krawczyk, 2018, Dynamic strain determination using fibre-optic cables allows imaging of seismological and structural features: Nature Communications, **9**, 2509, https://doi.org/10.1038/s41467-018-04860-y.

Lancelle, C., 2016, Distributed acoustic sensing for imaging near-surface geology and monitoring traffic at Garner Valley, California: Ph.D. Thesis, University of Wisconsin–Madison.

Lindsey, N. J., S. Yuan, A. Lellouch, L. Gualtieri, T. Lecocq, and B. Biondi, 2020, City-scale dark fiber DAS measurements of infrastructure use during the COVID-19 pandemic: Geophysical Research Letters, **47**, no. 16, https://doi.org/10.1029/2020GL089931.

Liu, H., J. Ma, W. Yan, W. Liu, X. Zhang, and C. Li, 2018, Traffic flow detection using distributed fiber optic acoustic sensing: IEEE Access, **6**, 68968–68980. https://doi.org/10.1109/ACCESS.2018.2868418.

Martin, E., N. Lindsey, S. Dou, J. Ajo-Franklin, T. Daley, B. Freifeld, M. Robertson, C. Ulrich, A. Wagner, and K. Bjella, 2016, Interferometry of a roadside DAS array in Fairbanks, AK: 86th Annual International Meeting, SEG, Expanded Abstracts, 2725–2729, https://doi.org/10.1190/segam2016-13963708.1.

Matzel, E., X. Zeng, C. Thurber, Y. Luo, and C. Morency, 2017, Seismic interferometry using the dense array at Brady Geothermal Field: Proceedings of the 42nd Workshop on Geothermal Reservoir Engineering, Stanford University, https://stanford.io/3l1ioqf, accessed 1 October 2020.

Miller, D. E., T. Coleman, X. Zeng, J. R. Patterson, E. C. Reinisch, M. A. Cardiff, H. F. Wang, et al., 2018, DAS and DTS at Brady Hot Springs: Observations about coupling and coupled interpretations: Proceedings of the 43rd Workshop on Geothermal Reservoir Engineering, Stanford University, https://stanford.io/2Sg3iRj, accessed 1 October 2020.

Mondanos, M., and T. Coleman, 2019, Application of distributed fibre-optic sensing to geothermal reservoir characterization and monitoring: First Break, **37**, no. 7, 51–56, https://doi.org/10.3997/1365-2397.n0040.

Patterson, J. R., M. Cardiff, T. Coleman, H. Wang, K. L. Feigl, J. Akerly, and P. Spielman, 2017, Geothermal reservoir characterization using distributed temperature sensing at Brady Geothermal Field, Nevada: The Leading Edge, **36**, no. 12, 1024a1–1024a7, https://doi.org/10.1190/tle36121024a1.1.

Wang, X., E. F. Williams, M. Karrenbach, M. G. Herraez, M. Fidalgo, and Z. Zhan, 2020, Rose Parade seismology: Signatures of floats and bands on optical fiber: Seismological Research Letters, **91**, no. 4, 2395–2398, https://doi.org/10.1785/0220200091.

Wu, W., Z. Yang, Q. Qin, and F. Hu, 2006, Adaptive seismic data compression using wavelet packets: IEEE International Symposium on Geoscience and Remote Sensing, https://doi.org/10.1109/IGARSS.2006.202.

Yuan, S., A. Lellouch, R. G. Clapp, and B. Biondi, 2020, Near-surface characterization using a roadside distributed acoustic sensing array: The Leading Edge, **39**, no. 9, 646–653, https://doi.org/10.1190/tle39090646.1.

Zeng, X., C. Thurber, H. Wang, D. Fratta, and E. Matzel, 2017, High-resolution shallow structure revealed with ambient noise tomography: Proceedings of the 42nd Workshop on Geothermal Reservoir Engineering, Stanford University.